Abrupt warming of the equatorial intermediate Pacific during Heinrich Stadial 1

Zhang Shuai [1, 2, 3], Li Tiegang [4, 5, *], Yu Zhoufei [3], Chang Fengming [2, 5], Gu Sifan [6], Xiong Zhifang [4, 5], Liu Heng [1], Qian Fang [2], Zhang Junru [2], Cheng Xuhua [1], Li Baohua [3, 5, *]

[1] College of Oceanography, Hohai University, Nanjing 210098, China
[2] Key Laboratory of Marine Geology and Environment, Institute of Oceanology, Chinese Academy of Sciences, Qingdao 266071, China
[3] State Key Laboratory of Palaeobiology and Stratigraphy, Nanjing Institute of Geology and Palaeontology, Chinese Academy of Sciences, Nanjing 210008, China
[4] Key Laboratory of Marine Geology and Metallogeny, First Institute of Oceanography, Ministry of Natural Resources, Qingdao 266061, China
[5] Laboratory for Marine Geology, Pilot National Laboratory for Marine Science and Technology (Qingdao), Qingdao 266237, China
[6] School of Oceanography, Shanghai Jiao Tong University, Shanghai 200240, China

* Corresponding authors : Tiegang Li, email address : tgli@fio.org.cn ; Baohua Li, email address : bh-li@nigpas.ac.cn

Abstract :

The Pacific intermediate water is essential for global ocean heat storage and transfer and connected to the higher latitude sea areas. Its thermohaline evolution and relationship to high latitudes on millennium scales, however, are both poorly understood. In this study, we used sediment core KX22–4 in the western equatorial Pacific to reconstruct the thermohaline and δ13C variations in the intermediate water over the past 28,000 years based on Mg/Ca, δ18O and δ13C measurements of deep dwelling planktonic foraminiferal species. The results show that during Heinrich Stadial 1, the temperature of intermediate water rapidly increased by roughly 6 °C and was simultaneous with the Southern Ocean surface water, carrying a typical Antarctic signature along with the salter and reduced δ13C signals. The Southern Hemisphere climatic development and the advection of the thermal anomaly into the tropical intermediate Pacific via the Southern Ocean intermediate water are thought to be closely coupled.

Highlights

► We reconstructed the thermohaline and δ13C variations of equatorial Pacific intermediate waters over the past 28,000 years. ► The temperature of the Pacific intermediate water rose by ~6 °C and accompanied by a salt enrichment in Heinrich Stadial 1. ► The thermohaline and δ13C of intermediate water show a temporal correspondence to Southern Ocean surface water.

1 Introduction

The reconstruction of intermediate water characteristics is crucial for understanding the changes in ocean heat and carbon transport in the Earth's climate system (Marshall and Speer, 2012). The warming "hiatus" in the surface ocean was intended, in the context of present global warming, to reflect a portion of the "lost" heat concealed by the ocean deep (Meehl et al., 2011). Recent observations demonstrated that the Southern Ocean absorbs three quarters of the extra heat produced by greenhouse gases, which is then transported northward to the ocean interior via the overturning circulation, changing the temperature and heat content of tropical intermediate water (Bourgeois et al., 2022). The change in water heat content in the tropical Pacific directly regulates the El Niño-Southern Oscillation, Pacific Decadal Oscillations, heat waves and typhoons in the northwest Pacific Ocean, affecting the climate change in the East Asia and possibly the entire world (Meehl et al., 2011; Cheng et al., 2022).

According to recent observations, the intermediate water in the equatorial Pacific is mainly originated from the subduction of Subantarctic mode water (SAMW) and Antarctic intermediate water (AAIW) (Toggweiler et al., 1991; Bostock et al., 2010; Bostock et al., 2013), which together make up the contemporary Southern Ocean intermediate water. While for the millennium events in the last deglaciation, the origin of the intermediate water in the equatorial Pacific is uncertain. According to some studies, the Atlantic meridional overturning circulation (AMOC) weakened or even collapsed during northern hemisphere cold events (McManus et al., 2004), Heinrich Stadial 1 (HS1, ~15.0–18.0 ka) and Younger Dryas (YD, ~12.9–11.7 ka), which reduced northward heat transport in the northern Atlantic and increased heat accumulation in the Southern Ocean

(Toggweiler and Lea, 2010), and the resulting surface warming was then entered the SAMW and

AAIW via northward subduction (Pahnke et al., 2008). Based on benthic foraminiferal proxies, the

intermediate waters of northern tropical Atlantic (Poggemann et al., 2018), southwestern Atlantic

(Umling et al., 2019) and northern Indian Ocean (Ma et al., 2020) experienced significant warming

in HS1, which was attributed to the invasion of the southern source water driven by an enhanced

Southern Ocean meridional circulation (Bryan et al., 2010; Poggemann et al., 2018; Yu et al., 2018).

Simulation results showed that during the HS1, warming induced southward southern atmosphere

westerlies would enhance Drake Passage upwelling and form a strong Ekman pumping, thereby

strengthening the supply of the Antarctic surface water to the AAIW (Downes et al., 2011).

Nevertheless, benthic foraminiferal Cd/Ca and ε_{Nd} records from the tropical Atlantic showed

suppressed and contractive AAIW, given its function as a return flow of the AMOC (Came et al.,

2008; Xie et al., 2012; Gu et al., 2017). Meanwhile, other studies have revealed that during HS1, an

augmented north Pacific intermediate water (NPIW) (Gray et al., 2018; Gong et al., 2019; Zou et

al., 2020) punctured southward even to south of Tasmania (Struve et al., 2022), as a "seesaw" in the

ventilation of the intermediate Atlantic and Pacific (Freeman et al., 2015). In the northwest

subtropical Pacific, two reconstructions observed fast warming intermediate water temperature

(IWT) during HS1 and interpreted it as a warming in the NPIW (Kubota et al., 2015; Yang et al.,

2020), but another reconstruction (Sagawa et al., 2011) recorded no quick IWT warming during

HS1. Only two IWTs from the Indonesian (Rosenthal et al., 2013) and eastern Pacific Oceans

(Kalansky et al., 2015) were recreated in the equatorial Pacific for the Holocene, which constrained

our understanding of the history of IWT in the tropical Pacific for a longer timescales.

In this study, temperature, salinity and $\delta^{13}C$ of the intermediate water in the western equatorial

Pacific were reconstructed using Mg/Ca and stable isotopes of deep dwelling planktonic foraminifera *Globorotalia crassaformis* and *Globorotalia truncatulinoides* dextral, with the goal of probing the thermohaline evolution of the western equatorial Pacific intermediate water during the last deglaciation and its potential linkages to high latitudes.

2 Oceanographic settings

The core site in this study is situated in the central western Pacific warm pool (Fig. 1), with a mean annual sea surface temperature (SST) exceeding 28.5°C. The intermediate water in the area is currently largely affected by the SAMW and AAIW (Toggweiler et al., 1991; Bostock et al., 2010; Bostock et al., 2013), with the NPIW occasionally having an impact (Struve et al., 2022). Most of the NPIW (300–700 m water depth, 34.2–34.3 psu, 26.7–26.8σ_θ) only reaches 7°N in the Philippine Sea because of the bifurcation latitude of North Equatorial Current and basin-wide wind forcing, although the south-sourced waters may reach 11°N (Talley, 2008; Wang et al., 2015). As they subduct equatorward from the mid-high latitude formation zones along the isopycnic, the SAMW and AAIW affect the thermohaline and nutrient properties of equatorial intermediate water largely from 500 to 1500 m water depth, with a salinity of 34.5–34.6 psu and a density of 27.2σ_θ (Bostock et al., 2010; Wang et al., 2015) (Fig. 1). As a result, the study area is a crucial location where north and south sources of water dispute.

3 Materials and Methods

3.1 Sediment samples

The sediment samples were collected with 1 cm interval from the giant piston Core KX22-4 (0.03°S, 159.24°E, Fig.1) recovered from the Ontong–Java Plateau during Cruise KX08-973 of the

R/V "Science-1 Vessel" (Zhang et al., 2017). The water depth is 2362 m, well above the lysocline in the equatorial Pacific, which is about 3.5 km (Parker and Berger, 1971). The core sediments are consisted of approximately 85% calcareous ooze, without obvious bioturbation (Zhang et al., 2017). This work focuses on the last deglacial interval that since 28 ka, and the age model was based on seven AMS ^{14}C dating points using planktonic foraminifera *Trilobatus sacculifer* (Tab. 1) (Zhang et al., 2017; Zhang et al., 2022).

3.2 Stable isotope and Mg/Ca analyses

Two subsurface planktonic foraminiferal species *G. crassaformis* and *G. truncatulinoides* dextral were picked for the reconstruction of intermediate waters. About 30 specimens per sample within a size fraction of 355–500 μm were prepared for stable isotope analyses and Mg/Ca measurements. Pretreatment and analysis procedures followed the method described by Zhang et al., 2017. For isotope measurements the crushed foraminiferal testes were treated with peroxide and acetone, and dried at 60°C. The oxygen and carbon isotopes were measured by Finnigan-MAT253 mass spectrometer equipped with an automatic carbonate preparation device (Kiel III) at the State Key Laboratory of Marine Geology, Tongji University with a standard deviation of 0.07‰. Isotope results were calibrated into PDB scale by the NBS-19 standard.

The Mg/Ca cleaning procedure followed the treating processes without a reductive step (Barker et al., 2003). The Mg/Ca ratio was measured using Inductively Coupled Plasma-Optical Emission Spectrometry (ICP-OES, Icap6300 radial; Thermo-Fisher) at the Institute of Oceanology, Chinese Academy of Science. The analytical precision of the Mg/Ca ratio was 0.44% (1σ, RSD). Al/Ca, Fe/Ca and Mn/Ca were measured alongside with Mg/Ca to monitor the cleaning efficiency. None of these ratios shows a correlation to Mg/Ca, indicating that the samples were not contaminated.

Furthermore, many studies from the warm pool have confirmed that the effect of salinity on Mg/Ca is negligible in this low salinity area (Arbuszewski et al., 2010; Hollstein et al., 2017). Based on the foraminiferal shell weight measurement of core KX22-4 (Zhang et al., 2021), no obvious dissolution effect was detected. Given the resistance to dissolution of *G. crassaformis* and *G. truncatulinoides* (Schiebel and Hemleben, 2017), the Mg/Ca-based temperature variations are robust.

3.3 Temperature and salinity reconstructions

Equation of Cléroux et al. (2011): Mg/Ca=0.78×exp (0.052×T) with an uncertainty of ±2°C and Zhang et al. (2022): Mg/Ca=0.69×exp (0.09×T) with an uncertainty of ±1°C were applied to calculate the temperature for *G. crassaformis* and *G. truncatulinoides*, respectively. They fit the temperature in situ very well (Fig. 2) (Zhang et al., 2021). The reconstructed Holocene IWTs from *G. crassaformis* and *G. truncatulinoides* match the published temperature records at comparable water depths based on benthic foraminifera from the eastern tropical Pacific (Kalansky et al., 2015) and Indonesian oceans (Rosenthal et al., 2013) (Fig. 3b).

The residual seawater $\delta^{18}O$ ($\delta^{18}O_{sw-iv}$) was calculated using the empirical equation T=16.5 - 4.8×(shell $\delta^{18}O$ (PDB) - seawater $\delta^{18}O$ (SMOW)) with a factor 0.27‰, which is the conversion from PDB to SMOW scale (Bemis et al., 1998). $\delta^{18}O_{sw-iv}$ might indicate the salinity fluctuation after the ice volume change (Spratt and Lisiecki, 2016) was corrected.

4   Results and Discussion

4.1 Variations of the temperature in the intermediate water

Based on the comparison of foraminiferal $\delta^{18}O$ values of the late Holocene samples (<5 ka) with the predicted $\delta^{18}O$ equilibrium values ($\delta^{18}O_{eq}$), the apparent calcification depths of crusted *G.*

crassaformis and *G. truncatulinoides* are at ~330 m and 540 m water depths, respectively (Zhang et al., 2022). The water depth from 300 to 700 m is also the main overlaps of intermediate waters from the north and the south (Bostock et al., 2010; Wang et al., 2015). No obvious vertical migration has been found in *G. crassaformis* (Cléroux and Lynch-Stieglitz, 2010) and *G. truncatulinoides* (Rebotim et al., 2019), and they could be used in paleoenvironment reconstruction of the intermediate water (Steph et al., 2009; Tapia et al., 2015).

Since the last deglacial period, the $\delta^{18}O$ fluctuation of deep dwelling species *G. crassaformis* and *G. truncatulinoides* has displayed a pattern that is quite distinct from those of surface water (*Globigerinoides ruber* and *T. sacculifer*) and thermocline species (*Pulleniatina obliquiloculata* and *Neogloboquadrina dutertrei*) (Fig. 3a). Deep dwelling species exhibited an opposite enriched $\delta^{18}O$ (~0.80‰) trend. In contrast to the continuous warming of the surface and thermocline waters during the deglaciation, the IWTs based on *G. crassaformis* and *G. truncatulinoides* rose rapidly in HS1 (about 6.0°C and 3.6°C warming with in 3.4 kyr interval, respectively, Fig. 3b; about 3.15°C and 2.12°C if the averages of time intervals of 14.76–17.00 ka and 18.15–19.30 ka were applied), which is significantly larger than the surface and thermocline warming (almost 1.1°C and 2.8°C, respectively).

Despite the absence of the direct deglacial IWT reconstruction in the equatorial Pacific, this substantial warming in the intermediate water of equatorial Pacific during HS1 is also observed in the intermediate waters of the northern Indian Ocean (7.5°N, 1,254 m water depth) (Ma et al., 2020) and western tropical Atlantic (~11°N, 852 m water depth) (Poggemann et al., 2018). Benthic foraminiferal Mg/Li increased by 1.1mol/mmol, equivalent to ~5.5°C warming during HS1 in the northern Indian Ocean (Ma et al., 2020), which is compatible with reconstructions made in the

southwest Atlantic (~27°S, 1,108–1,268 m) (Umling et al., 2019). In the meantime, the benthic foraminiferal Mg/Ca recorded a ~6.0°C warming in the western tropical Atlantic (Poggemann et al., 2018) and northwest Atlantic (~49°N, 1,251 m water depth) (Marcott et al., 2011). Based on the Mg/Ca of *G. truncatulinoides,* a 3°C warming in the 150–450 m depth during HS1 was also detectable in the south Pacific (~46°S) (Tapia et al., 2015). Additionally, the average vertical thermal gradients, the temperature difference between the surface and thermocline water (ΔT_{upper}) and between the thermocline and intermediate water (ΔT_{lower}), decreased during HS1 (Fig. 3b), partly as a result of the fast warming in the ocean internal. This indicate that during HS1, when the northern hemisphere was cold, the interior equatorial Pacific was storing heat as the Southern Ocean (Toggweiler and Lea, 2010; Riethdorf et al., 2013; Gray et al., 2018; Praetorius et al., 2020). The global ocean heat content, which was reconstructed using ice core inert gas records, likewise showed an increase in the ocean heat content during HS1 (Baggenstos et al., 2019).

The different evolutions of intermediate waters from the upper waters illustrate that the intermediate water would more closely mirror the properties of higher latitude source regions (Wong et al., 1999). In this study, the IWT data from core KX22-4 were compared to the SST records in high latitude source areas in the northwest Pacific (Riethdorf et al., 2013; Gray et al., 2018), northeast Pacific (Praetorius et al., 2020) and southeast Pacific (Haddam et al., 2018) (Fig.1, 4a-d). The equatorial Pacific IWT records revealed an Antarctic-style HS1 warming (Fig. 4c). At the beginning of HS1 (about 18 ka), temperatures in the southeast Pacific surface and western equatorial Pacific intermediate water both started to rise synchronously and peaked around the same time (about 15 ka), with a similar temperature fluctuation of 6°C. Although a similar SST rise was seen in the north high latitude during the HS1, it temporally lagged and started at ~16 ka and peaked at

~14.5 ka (Fig. 4a, b). Similarly, no discernible warming was found even in the northwest Pacific

intermediate waters (Sagawa et al., 2011). Warming of AAIW in the tropical western Atlantic during

HS1 and YD were induced by major AMOC perturbations resulting in the pronounced accumulation

of heat in the surface Southern Ocean (Poggemann et al., 2018). Previous studies also argued for

the transfer of the Southern Ocean surface temperature signature via intermediate waters into 7°S

in the western Indian Ocean (Romahn et al., 2014). Nonetheless, the deeper IWT reconstructed by

G. truncatulinoides abruptly declined at the height of the shallow one induced by *G. crassaformis*

(Fig. 4c). The shallow one is more impacted by subtropical water mixing than the deeper one, which

is more affected by the Southern Ocean's higher latitude. Higher latitude source regions would be

more sensitive and show earlier change during the evolution of the Southern Ocean, resulting in

phase diversity between the IWT reconstructions from *G. truncatulinoides* and *G. crassaformis*.

Furthermore, near the end or latter part of HS1, the increased and warmer shallow NPIW would

augment tropical warming (Fig. 4a, b), mismatching the deeper reconstruction.

4.2 The southern influence to the intermediate water

The $\delta^{18}O_{sw-iv}$ reconstructions from *G. crassaformis* and *G. truncatulinoides* at core KX22-4

showed a 1.37–1.90‰ enrichment during HS1 (Fig. 4g), indicating a rapid rise in salinity as the

temperature rose. It might represent a source water replenishment with high salinity and temperature

in HS1. As the subducted waters transport along the isopycnic surface, similar changes should occur

upstream and downstream of the water mass, as the same fluctuations in temperature (~6°C) and

$\delta^{18}O_{sw-iv}$ (~2.0‰). Similar to the temperature, the southeast Pacific surface water displayed an

isochronous salifying (~2.0‰) (Haddam et al., 2020) with the equatorial intermediate water, while

the salifying in northwest Pacific surface (Riethdorf et al., 2013) lagged (Fig. 4f). The enrichment

of $\delta^{18}O$ of *G. crassaformis* and *G. truncatulinoides* (Fig. 3a) during HS1 suggested that salinity

played a more important role than temperature in forcing the subduction of the warm, salty surface

water from high latitudes to the equatorial Pacific, as shown by the TraCE model (Liu et al., 2009)

in Fig. 5a that a strong positive salinity anomaly existed in the south Pacific at 500 m water depth

in HS1. This is also demonstrated by a 2.0‰ $\delta^{18}O_{sw-iv}$ enrichment (lose of buoyancy) in the sea

surface salinity of the southeast Pacific. When the southern Pacific subtropical gyres moved

southward, it could cause the mid-high latitude subduction zones to become warmer and saltier

during HS1 (Chiang et al., 2018) and amplify our proxies reconstruction of intermediate water.

The $\delta^{13}C$ of intermediate water species *G. crassaformis* and *G. truncatulinoides* in core KX22-

4 showed depleted values during HS1 (Fig. 4k), and this signal has been noted widely from the high

to low latitudes, and has been treated as a global signal that primarily originates from the deep ocean

ventilation or air-sea exchange. On the one hand, the outgassing in the western equatorial Pacific

during HS1 as seen by the positive pCO_2 (Fig. 4j) (Palmer and Pearson, 2003) would hamper the

depleted $\delta^{13}C$ signal from the atmosphere to the ocean. On the other hand, the nearby productivity

(Liang and Liu, 2016) was elevated during HS1 (Fig. 4l), which would increase $\delta^{13}C$ value of the

upper water and be in contrast with our records (Fig. 4k). As a result, we believe that the deep ocean

ventilation is more likely to be responsible for this depleted $\delta^{13}C$ signal.

A number of depleted $\Delta^{14}C$ and $\delta^{13}C$ records from eastern equatorial Pacific (Stott et al., 2009;

de la Fuente et al., 2015; Chen et al., 2020) and off the coast of Baja California (Marchitto et al.,

2007; Basak et al., 2010; Sánchez and Carriquiry, 2022) suggested a significant increase in

thermocline and intermediate water intrusion from the south. Besides, the low-latitude Pacific has

experienced a decline in the influence of northern intermediate water masses since ~17 ka, according

to the $\delta^{13}C$ and εNd signatures of benthic foraminifera (Max et al., 2017). A reduction in seawater

$\delta^{18}O$ and SST during HS1 was also predicted by diatomic $\delta^{18}O$ data from the northeast Pacific,

which would be harmful to the NPIW subduction (Maier et al., 2018). Our intermediate water $\delta^{13}C$

data and *Globorotalia inflata* $\delta^{13}C$ record from the southwest Pacific (Schiraldi et al., 2014) (Fig.

4m) both showed a 0.4‰ decrease during HS1. Covariations in $\delta^{13}C$ (Stott et al., 2009) and $\Delta^{14}C$

(Basak et al., 2010) between the equatorial Pacific and the Southern Ocean suggest thermocline and

intermediate layer penetration during HS1. According to the findings on an isotope enabled ocean

model with various geotracers ($\delta^{13}C$, εNd, $^{231}Pa/^{230}Th$, $\delta^{18}O$ and $\Delta^{14}C$) (Gu et al., 2020), more AAIW

occupied the 500–700 m water depth in the equatorial western Pacific during HS1 than the last

glacial maximum and Antarctic Cold Reversal (14.7–12.9 ka) (Fig. 6). When the Southern Ocean

overturning circulation increased during HS1, ^{14}C rich deep water may be transported to the

Southern Ocean surface and equator (Ronge et al., 2021a). The radiocarbon depleted intermediate

waters and significant $\delta^{13}C_{atm}$ depletion of atmospheric CO_2 during HS1 (Fig. 4i) were caused by

enhanced upwelling of a long isolated carbon reservoir (Romahn et al., 2014). Meanwhile, the

warmer IWT would diminish the solubility of oceanic CO_2, contributing to deep CO_2 release and

driving the global greenhouse warming (Palmer and Pearson, 2003). Additionally, the depleted $\delta^{13}C$

observed in the surface and thermocline waters was speculated to reflect the isotopic signal of the

upwelled underlying intermediate water (Oppo and Fairbanks, 1989; Linsley and Dunbar, 1994; Li

et al., 2002).

Following the HS1, all reconstructed IWTs declined during the Antarctic Cold Reversal, but

the ΔTs climbed (Fig. 3b), which might be attributed to a decrease in heat input and/or an increase

in internal thermal release. During the Antarctic Cold Reversal, the IWT cooled almost

simultaneously with the SST cooling in the southeast Pacific (Fig. 4c, d). Global sea level calculation revealed that a significant rate of sea level rise occurred during a 500-year period around 14.6 ka, which was mostly attributable to an Antarctic meltwater pulse (Weaver et al., 2003). This would freshen the Southern Ocean's surface water while weakening the AAIW formation and its relevant source of the low-latitude intermediate water.

During the YD, both IWTs and ΔTs failed to detect secondary warming in the Southern Ocean. This may be owing to the poor resolution of our sample, but an IWT based on *G. crassaformis* revealed a modest warming trend from 13 to 10 ka. Such weaker intermediate water warming at low latitude in YD is also observed in IWT reconstructions from the subtropical to tropical western Atlantic (Poggemann et al., 2018; Umling et al., 2019) and northern Indian Ocean (Ma et al., 2020). The intermediate water $\delta^{18}O_{sw-iv}$ data indicated a reduction across the YD period, correlating to a decrease in surface water salinity in the southeast Pacific (Fig. 4g, h). This would weaken subduction and result in a temperature difference signal, indicating that IWT at core KX22-4 did not detect the warming signal from the south (Fig. 4c). According to $\Delta^{14}C$ data from the northern Arabian Sea, the age of the intermediate water during YD is younger than that during HS1, suggesting a relatively week penetration during YD (Bryan et al., 2010). The εNd signals from Indian Ocean (Yu et al., 2018), Atlantic Ocean (Pahnke et al., 2008) and Pacific Ocean (Basak et al., 2010) likewise exhibited a lower AAIW in the YD than HS1, with the Pacific showing the greatest decrease (Basak et al., 2010). TraCE model results predicted lower seawater salinity and density in YD than HS1 at 500 m water depth in the south Pacific (Liu et al., 2009) (Fig. 5). When compared to HS1, the AMOC dropped less during YD (McManus et al., 2004; Ritz et al., 2013), indicating less overturning in the Southern Ocean (Siani et al., 2013; Dumont et al., 2020) (Fig. 4n). The $^{231}Pa/^{230}Th$

and $\Delta\Delta^{14}C$ data suggested that the south Pacific overturning circulation peaked during HS1 (Ronge et al., 2021b). Furthermore, meltwater episodes in the Southern Ocean triggered by higher sea level and warmer YD may limit the production of SAMW and AAIW.

In addition, because of the low sedimentation rate in the sampling location, our results of millennia scale fluctuations are subjected to inaccuracy. The likelihood of mechanical disturbances (such as bioturbation and winnowing) harmed the results of this study, which must be emphasized in any citations or discussions. The possible present of bioturbation implies that the amplitude of temperature rise during HS1 may larger than observed in this study, while it will not affect the observed rising trend which involves 5–6 data points step by step for both species. More research is required in this area to test the reconstruction of the intermediate water.

5 Conclusions

$\delta^{18}O$, $\delta^{13}C$ and Mg/Ca ratio of deep dwelling planktonic foraminifera *G. crassaformis* and *G. truncatulinoides* were analyzed from core KX22-4 in the equatorial western Pacific, in order to reconstruct the evolution of the intermediate water since 28 ka. The findings indicated that high latitude millennial-scale events might leave an impression on the equatorial Pacific intermediate water and alter its inner water properties. The ocean's interior was significantly charged during the HS1, the northern hemisphere cooling interval, and contributed to the global warming during the later portion of the deglaciation. Meanwhile, the strengthening of the Southern Ocean overturning circulation resulted in the release of old respired carbon from the deep, further amplifying the greenhouse effect. We hypothesize that if global warming continues, heat absorption in the Southern Ocean would enhance the warming of the ocean interior and cause more carbon to enter the atmosphere, accelerating the global warming.

Data Availability Statement

The data are available at Pangaea (https://doi.pangaea.de/10.1594/PANGAEA.947087) and the supporting materials. Model data used to produce the results in this study can be obtained from https://zenodo.org/record/7260087 (doi:10.5281/zenodo.7260087). Codes for TRACE are publicly available at https://www.earthsystemgrid.org/project/trace.html.

Tab. 1. Radiocarbon dates of core KX22-4 (Zhang et al., 2017; Zhang et al., 2022). The radiocarbon ages were converted to calendar ages using the CALIB 8.1.0 program and updated MARINE20 calibration (Heaton et al., 2020), taking the local reservoir ($\Delta R=20\pm177$ yr) from the most-nearby ages of modern seawater (http://calib.org/marine) into account.

| Depth (cm)	Lab code	Uncorrected ^{14}C age (yr B.P. ±1σ)	Local reservoir (ΔR) (yr, ±1σ)	Calendar age (yr B.P.)	Range (1σ) (yr B.P.)
5-6	OS-101065	4120±25	20±177	3964	3717-4210
13-14	OS-101066	5770±25	20±177	5961	5755-6167
26-27	OS-101067	9820±25	20±177	10569	10300-10838
30-31	Beta-566811	12610±40	20±177	14042	13755-14328
35-36	Beta-566812	13840±40	20±177	15849	15597-16102
39-40	OS-101068	17700±65	20±177	20448	20214-20682
49-50	OS-101081	23800±85	20±177	27160	26985-27334
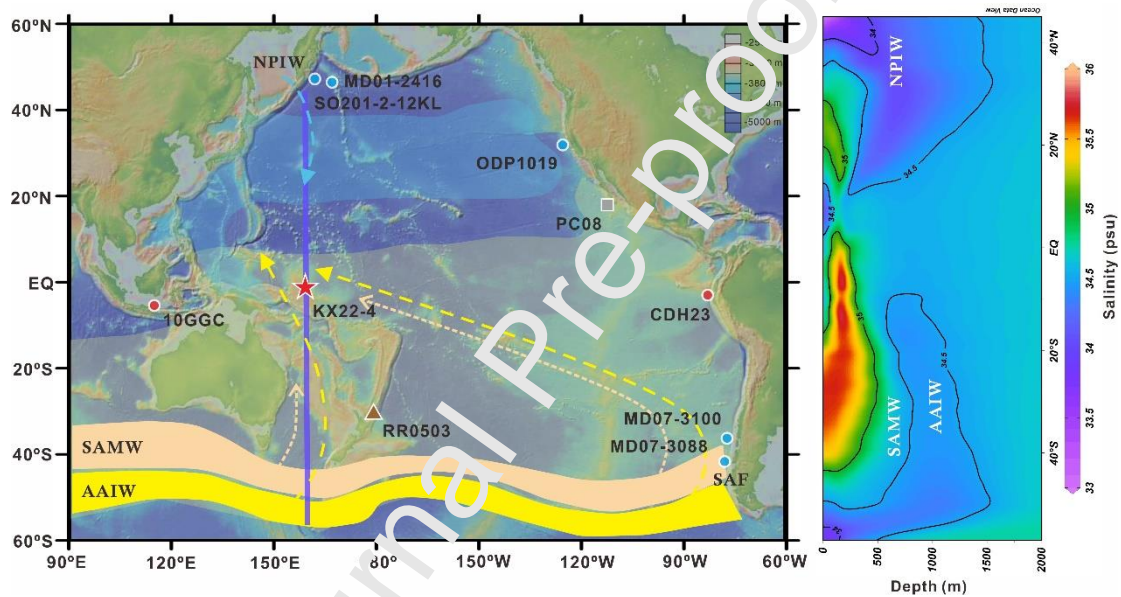
Fig. 1. The distribution of intermediate waters in the modern Pacific Ocean. The yellow and sand bands in the

left panel represent the formation zones of the Antarctic intermediate water (AAIW) and Subantarctic mode water

(SAMW) in the Southern Ocean, respectively, and the transparent yellow area marks the regions under their influence.

The blue transparent area marks the modern extent of the north Pacific intermediate water (NPIW) (Talley, 2008).

The dashed lines indicate possible transmission paths of intermediate waters. The red star represents the location of

core KX22-4 in this study. The red circles mark intermediate water temperature records within the Holocene. The

blue cycles mark the sea surface temperature records for comparison. The brown triangle represents the location of

the *G. inflata* δ^{13}C data. Gray square represents the location of the Δ^{14}C data. The map is a Mercator projection

generated by the online map generator at http://www.geomapapp.org/MSInstall.html. The right panel shows a

meridional salinity profile marked as the bold blue line in the left panel, which is created using Ocean Data View

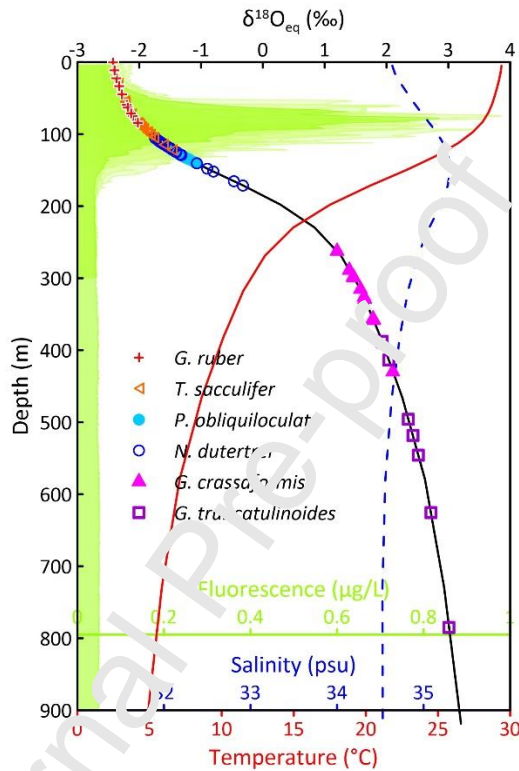(Schlitzer, 2015) based on the World Ocean Atlas 2018 salinity data (Zweng et al., 2018).

Fig. 2. The calcification depth estimated (Zhang et al., 2022). The temperature and salinity data are come from

SODA reanalysis dataset (v2.2.4, http://apdrc.soest.hawaii.edu/datadoc/soda_2.2.4.php). The predicted $\delta^{18}O_{eq}$ then

were calculated by the empirical equation $SST = 16.9 - 4.38 \times (\delta^{18}O_{eq} - \delta^{18}O_{sw} + 0.27) + 0.1 \times (\delta^{18}O_{eq} - \delta^{18}O_{sw} + 0.27)^2$

(Shackleton, 1974). The chlorophyll concentration data are combined the in situ data from 155°E-165°E, 2°S-2°N
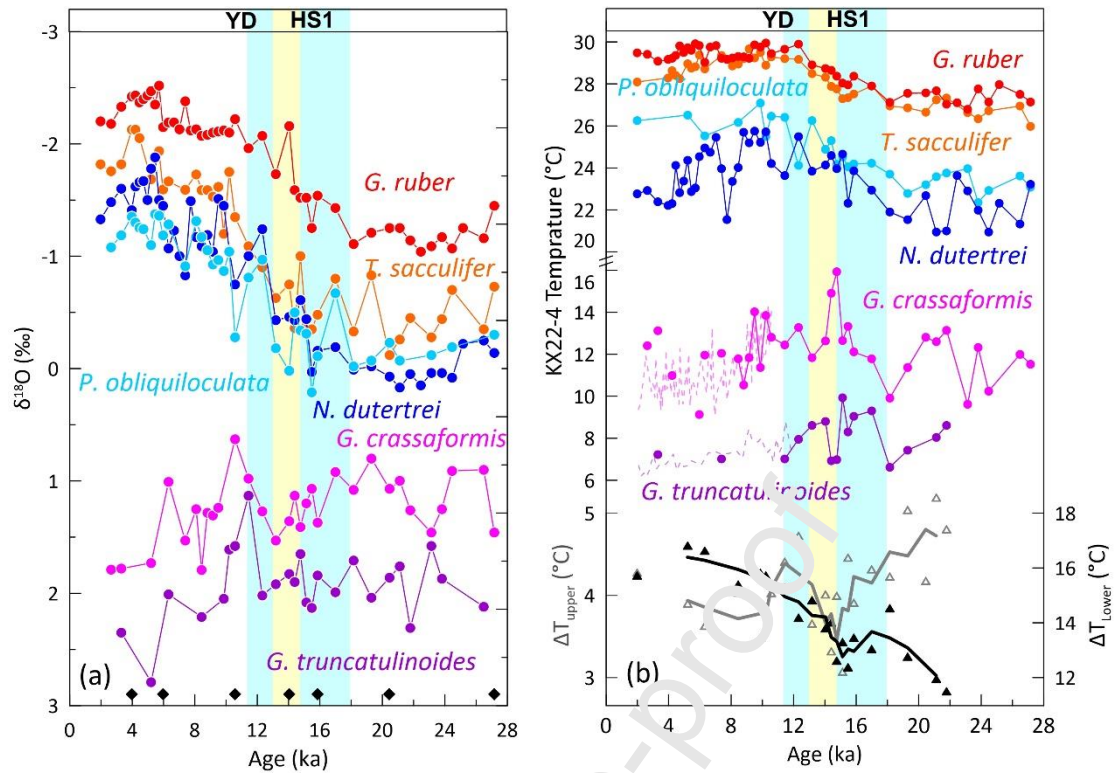
(Bonnet et al., 2009).

Fig. 3. δ¹⁸O and seawater temperature reconstructions based on planktonic foraminifera dwelling at various water layers at core KX22-4 in western equatorial Pacific. (a) δ¹⁸O records of surface water (*G. ruber* and *T. sacculifer*) (Zhang et al., 2017; Zhang et al., 2022), thermocline water (*N. dutertrei* and *P. obliquiloculata*) (Zhang, 2016; Zhang et al., 2021) and intermediate waters (*G. crassaformis* and *G. truncatulinoides*) (this study). Black diamonds mark the AMS ¹⁴C dating points. (b) Seawater temperatures based on Mg/Ca of multiple planktonic foraminifera (Zhang, 2016; Zhang et al., 2022), as well as the vertical temperature difference between the surface and thermocline water mean values (ΔT_upper) (gray triangles), and between the thermocline and intermediate water mean values (ΔT_lower) (black triangles). The gray and black lines are three point moving averages. The dashed lines in magenta and purple represent published IWT reconstructions from 374 m water depth in the eastern tropical Pacific (Kalansky et al., 2015) and 649 m water depth in Indonesian oceans (Rosenthal et al., 2013) based on benthic foraminifera, respectively.
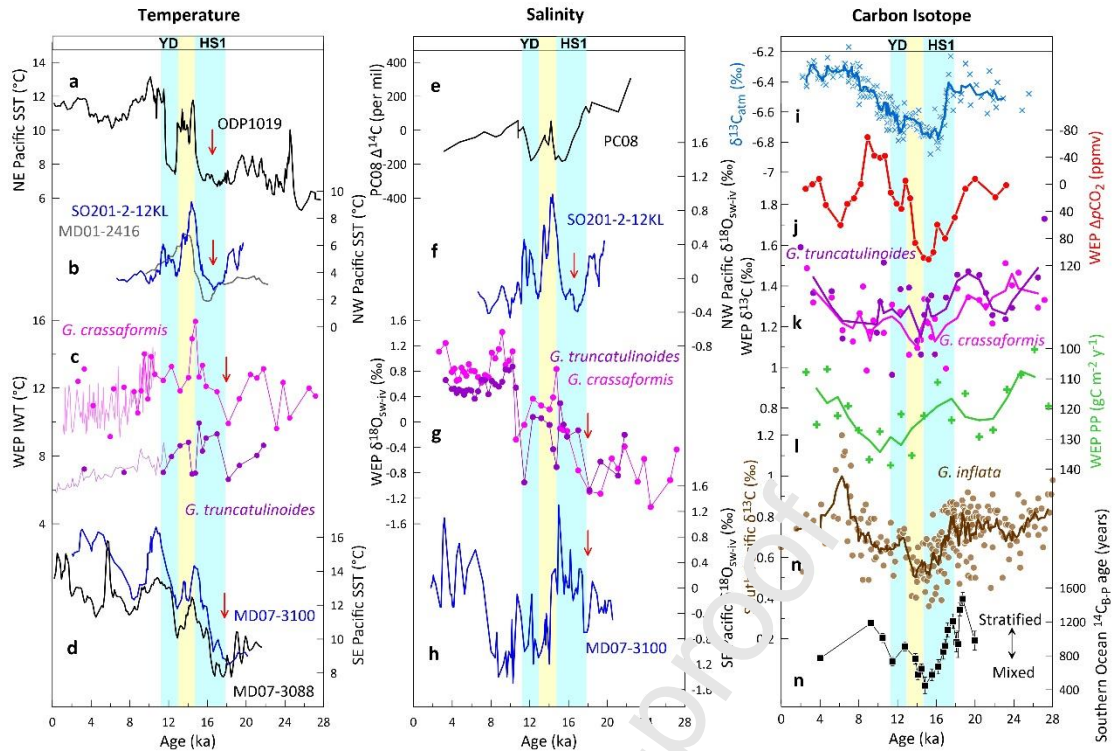
Fig. 4. Comparisons of the temperature, salinity and δ¹³C records of the intermediate water from the western equatorial Pacific (WEP) with published records in the northern and southern high latitudes. The cores include ODP1019 in the northeast Pacific (Praetorius et al., 2020) (a), SO201-2-12KL and MD01-2416 in the northwest Pacific (Riethdorf et al., 2013; Gray et al., 2018) (b, f), KX22-4 in the WEP (c, g, k) and MD07-3100 and MD07-3088 in the southeast Pacific (Haddam et al., 2018) (d, h). The Δ¹⁴C data comes from core PC08 on the open margin off the west coast of southern Baja California (Marchitto et al., 2007) (e). Atmospheric δ¹³C derived from Antarctic ice cores (Schmitt et al., 2012) (i). Calculated $\Delta p\text{CO}_2$ between the surface water and atmospheric $p\text{CO}_2$ from core ERDC-92 in the western equatorial Pacific (WEP) (Palmer and Pearson, 2003) (j). Reconstructed primary productivity (PP) from core KX21-2 (157.98° E, 1.42° S) in the western equatorial Pacific (Liang and Liu, 2016) (l).δ¹³C of *G. inflata* from the southwest Pacific (Schiraldi et al., 2014) (m). Ventilation ages (¹⁴C$_{\text{B-P}}$) from Core MD07-3088 in the southeast Pacific as a proxy of Southern Ocean ventilating intensity (Siani et al., 2013) (n). The red arrows in the panels reflect the approximate times when the increases begin.
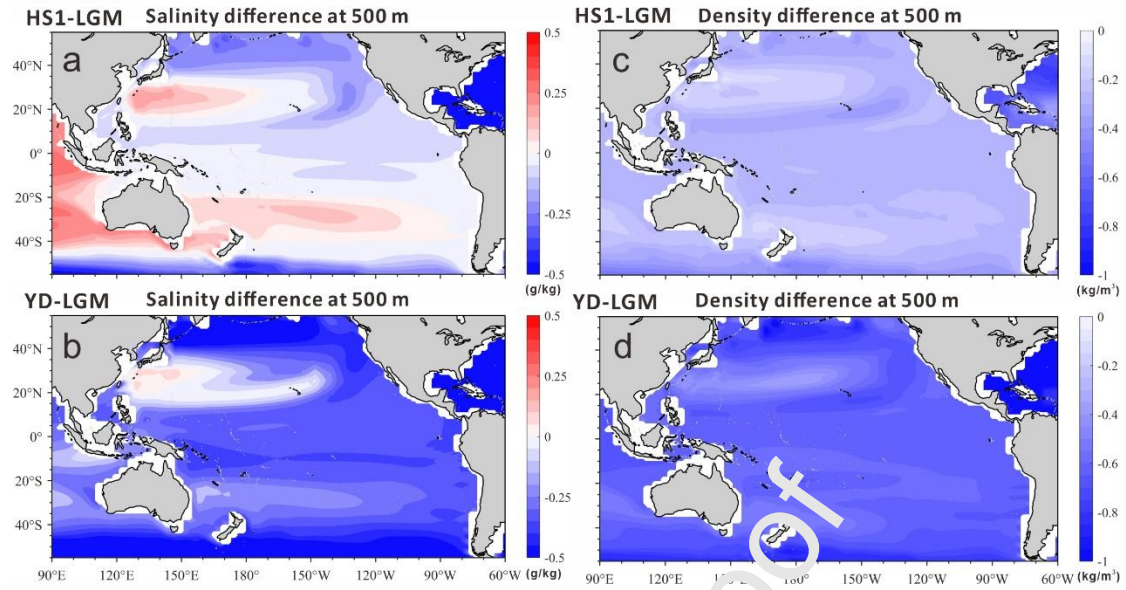
Fig. 5. Modeled salinity (a, b) and density (c, d) differences in HS1 (15 ka) and YD (12 ka) compared to LGM

(20 ka) at 500 m water depth by TraCE model (Liu et al., 200...).
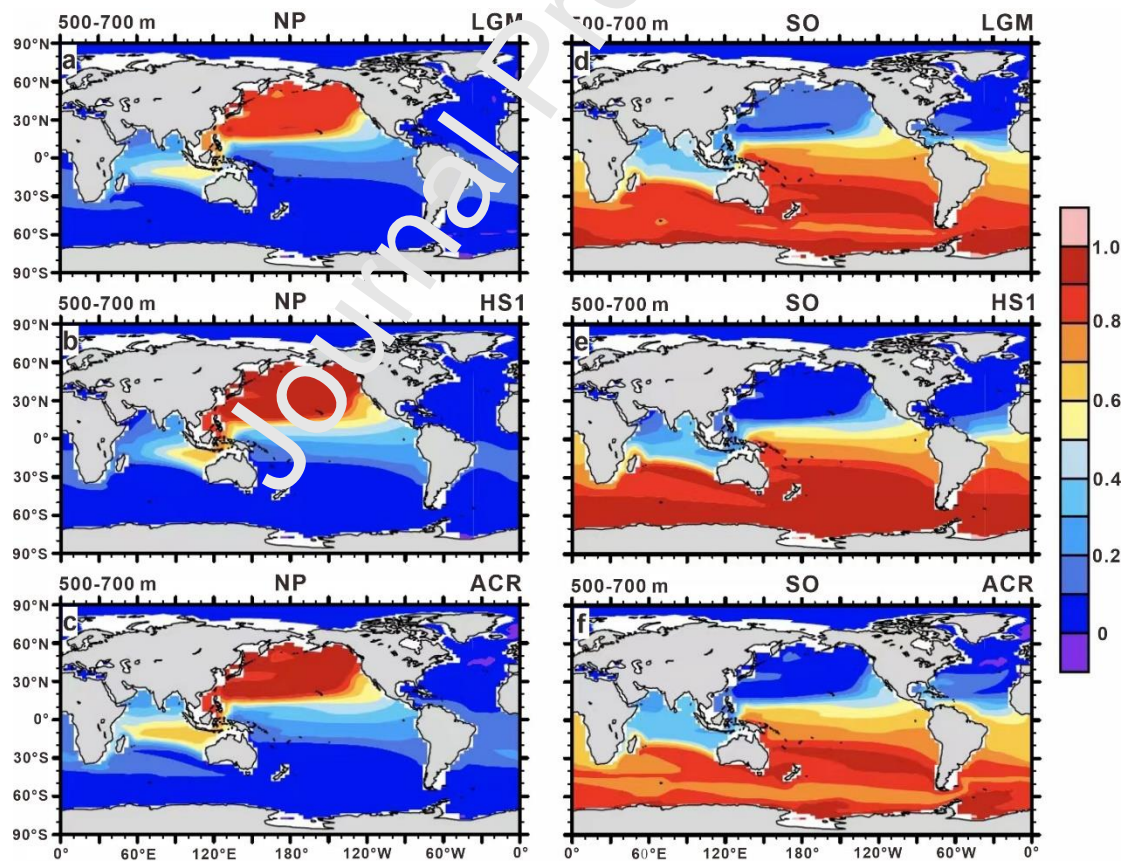

Fig. 6. The proportion of water masses from the north Pacific (NP) (a－c) and Southern Ocean (SO) (d－f) at

500－700 m water depth during the last glacial maximum (LGM), Heinrich Stadial 1 (HS1) and Antarctic

Cold Reversal (ACR) modeled by C-iTraCE (Gu et al., 2020). The identification of the distribution of water

masses is facilitated by passive dye tracers, which released at surface and fixed with the value at 1 in the SO and 0

outside SO for SO dye (right) and fixed at 1 at NP and 0 outside NP for NP dye (left) (Gu et al., 2020).

References

Arbuszewski, J., deMenocal, P., Kaplan, A., Farmer, E.C., 2010. On the fidelity of shell-derived $\delta^{18}O_{seawater}$ estimates. Earth Planet. Sci. Lett. 300, 185–196.

Baggenstos, D., Häberli, M., Schmitt, J., Shackleton, S.A., Birner, B., Severinghaus, J.P., Kellerhals, T., Fischer, H., 2019. Earth's radiative imbalance from the Last Glacial Maximum to the present. Proc. Natl Acad. Sci. USA 116, 14881–14886.

Barker, S., Greaves, M., Elderfield, H., 2003. A study of cleaning procedures used for foraminiferal Mg/Ca paleothermometry. Geochemistry Geophysics Geosystems 4, 8407.

Basak, C., Martin, E.E., Horikawa, K., Marchitto, T.M., 2010. Southern Ocean source of ^{14}C-depleted carbon in the North Pacific Ocean during the last deglaciation. Nat. Geosci. 3, 770–773.

Bemis, B.E., Spero, H.J., Bijma, J., Lea, D.W., 1998. Reevaluation of the oxygen isotopic composition of planktonic foraminifera: experimental results and revised paleotemperature equations. Paleoceanography 13, 150–160.

Bonnet, S., Biegala, I.C., Dutrieux, P., Slemons, L.O., Capone, D.G., 2009. Nitrogen fixation in the western equatorial Pacific: rates, diazotrophic cyanobacterial size class distribution, and biogeochemical significance. Global Biogeochemical Cycles 23, GB3012.

Bostock, H.C., Opdyke, B.N., Williams, M.J.M., 2010. Characterising the intermediate depth waters of the Pacific Ocean using $\delta^{13}C$ and other geochemical tracers. Deep Sea Res., Part I 57, 847–859.

Bostock, H.C., Sutton, P.J., Williams, M.J.M., Opdyke, B.N., 2013. Reviewing the circulation and mixing of Antarctic Intermediate Water in the South Pacific using evidence from geochemical tracers and Argo float trajectories. Deep Sea Res., Part I 73, 84–98.

Bourgeois, T., Goris, N., Schwinger, J., Tjiputra, J.F., 2022. Stratification constrains future heat and carbon uptake in the Southern Ocean between 30° S and 55° S. Nature Communications 13, 340.

Bryan, S.P., Marchitto, T.M., Lehman, S.J., 2010. The release of ^{14}C-depleted carbon from the deep ocean during the last deglaciation: Evidence from the Arabian Sea. Earth Planet. Sci. Lett. 298, 244–254.

Came, R.E., Oppo, D.W., Curry, W.B., Lynch-Stieglitz, J., 2008. Deglacial variability in the surface return flow of the Atlantic meridional overturning circulation. Paleoceanography 23.

Chen, T., Robinson, L.F., Burke, A., Claxton, L., Hain, M.P., Li, T., Rae, J.W.B., Stewart, J., Knowles, T.D.J., Fornari, D.J., Harpp, K.S., 2020. Persistently well-ventilated intermediate-depth ocean through the last deglaciation. Nat. Geosci. 13,

733–738.

Cheng, L., Abraham, J., Trenberth, K.E., Fasullo, J., Boyer, T., Mann, M.E., Zhu, J., Wang, F., Locarnini, R., Li, Y., Zhang, B., Tan, Z., Yu, F., Wan, L., Chen, X., Song, X., Liu, Y., Reseghetti, F., Simoncelli, S., Gouretski, V., Chen, G., Mishonov, A., Reagan, J., 2022. Another Record: Ocean Warming Continues through 2021 despite La Niña Conditions. Advances in Atmospheric Sciences 39, 373–385.

Chiang, J.C.H., Tokos, K.S., Lee, S.Y., Matsumoto, K., 2018. Contrasting Impacts of the South Pacific Split Jet and the Southern Annular Mode Modulation on Southern Ocean Circulation and Biogeochemistry. Paleoceanogr. Paleoclimatol. 33, 2–20.

Cléroux, C., Lynch-Stieglitz, J., 2010. What caused G. truncatulinoides to calcify in shallower water during the early Holocene in the western Atlantic/Gulf of Mexico? IOP Conference Series: Earth and Environmental Science 9, 012020.

de la Fuente, M., Skinner, L., Calvo, E., Pelejero, C., Cacho, I., 2015. Increased reservoir ages and poorly ventilated deep waters inferred in the glacial Eastern Equatorial Pacific. Nature Communications 6, 7420.

Downes, S.M., Budnick, A.S., Sarmiento, J.L., Farneti, R., 2011. Impacts of wind stress on the Antarctic Circumpolar Current fronts and associated subduction. Geophys. Res. Lett. 38, L11605.

Dumont, M., Pichevin, L., Geibert, W., Crosta, X., Michel, E., Moreton, S., Dobby, K., Ganeshram, R., 2020. The nature of deep overturning and reconfigurations of the silicon cycle across the last deglaciation. Nature Communications 11, 1534.

Freeman, E., Skinner, L.C., Tisserand, A., Dokken, T., Timmermann, A., Menviel, L., Friedrich, T., 2015. An Atlantic–Pacific ventilation seesaw across the last deglaciation. Earth Planet. Sci. Lett. 424, 237–244.

Gong, X., Lembke-Jene, L., Lohmann, G., Knorr, G., Tiedemann, R., Zou, J.J., Shi, X.F., 2019. Enhanced North Pacific deep-ocean stratification by stronger intermediate water formation during Heinrich Stadial 1. Nature Communications 10, 656.

Gray, W.R., Rae, J.W.B., Wills, R.C.J., Shevenell, A.E., Taylor, B., Burke, A., Foster, G.L., Lear, C.H., 2018. Deglacial upwelling, productivity and CO_2 outgassing in the North Pacific Ocean. Nat. Geosci. 11, 340–344.

Gu, S., Liu, Z., Oppo, D.W., Lynch-Stieglitz, J., Jahn, A., Zhang, J., Wu, L., 2020. Assessing the potential capability of reconstructing glacial Atlantic water masses and AMOC using multiple proxies in CESM. Earth Planet. Sci. Lett. 541, 116294.

Gu, S., Liu, Z., Zhang, J., Rempfer, J., Joos, F., Oppo, D.W., 2017. Coherent response of Antarctic Intermediate Water and Atlantic Meridional Overturning Circulation during the last deglaciation: reconciling contrasting neodymium isotope reconstructions from the tropical Atlantic. Paleoceanography 32, 1036–1053.

Haddam, N.A., Michel, E., Siani, G., Licari, L., Dewilde, F., 2020. Ventilation and Expansion of Intermediate and Deep Waters in the Southeast Pacific During the Last Termination. Paleoceanogr. Paleoclimatol. 35, e2019PA003743.

Haddam, N.A., Siani, G., Michel, E., Kaiser, J., Lamy, F., Duchamp-Alphonse, S., Hefter, J., Braconnot, P., Dewilde, F., Isgüder, G., Tisnerat-Laborde, N., Thil, F., Durand, N., Kissel, C., 2018. Changes in latitudinal sea surface temperature gradients along the Southern Chilean margin since the last glacial. Quat. Sci. Rev.

194, 62–76.

Heaton, T.J., Köhler, P., Butzin, M., Bard, E., Reimer, R.W., Austin, W.E.N., Bronk Ramsey, C., Grootes, P.M., Hughen, K.A., Kromer, B., Reimer, P.J., Adkins, J., Burke, A., Cook, M.S., Olsen, J., Skinner, L.C., 2020. MARINE20—The Marine radiocarbon age calibration curve (0–55,000 cal BP). Radiocarbon 62, 779–820.

Hollstein, M., Mohtadi, M., Rosenthal, Y., Moffa Sanchez, P., Oppo, D., Martínez Méndez, G., Steinke, S., Hebbeln, D., 2017. Stable oxygen isotopes and Mg/Ca in planktic foraminifera from modern surface sediments of the western Pacific warm pool: implications for thermocline reconstructions. Paleoceanography 32, 1174–1194.

Kalansky, J., Rosenthal, Y., Herbert, T., Bova, S., Altabet, M., 2015. Southern Ocean contributions to the eastern equatorial Pacific heat content during the Holocene. Earth Planet. Sci. Lett. 424, 158–167.

Kubota, Y., Kimoto, K., Itaki, T., Yokoyama, Y., Miyairi, Y., Matsuzaki, H., 2015. Bottom water variability in the subtropical northwestern Pacific from 26 kyr BP to present based on Mg/Ca and stable carbon and oxygen isotopes of benthic foraminifera. Clim. Past 11, 803–824.

Li, T., Liu, Z., Hall, M.A., Saito, Y., Berne, S., Cang, S., Cheng, Z., 2002. A broad deglacial $\delta^{13}C$ minimum event in planktonic foraminiferal records in the Okinawa Trough. Chinese Science Bulletin 47, 599–603.

Liang, D., Liu, C., 2016. Variations and controlling factors of the coccolith weight in the Western Pacific Warm Pool over the last 200 ka. Journal of Ocean University of China 15, 456–464.

Linsley, B.K., Dunbar, R.B., 1994. The Late Pleistocene history of surface water $\delta^{13}C$ in the Sulu Sea: Possible relationship to Pacific Deepwater $\delta^{13}C$ changes. Paleoceanography 9, 317–340.

Liu, Z., Otto-Bliesner, B.L., He, F., Brady, E.C., Tomas, R., Clark, P.U., Carlson, A.E., Lynch-Stieglitz, J., Curry, W., Brook, E., Erickson, D., Jacob, R., Kutzbach, J., Cheng, J., 2009. Transient simulation of last deglaciation with a new mechanism for Bølling-Allerød warming. Science 325, 310–314.

Ma, R., Sépulcre, S., Bassinot, F., Haurine, F., Tisnérat-Laborde, N., Colin, C., 2020. North Indian Ocean Circulation Since the Last Deglaciation as Inferred From New Elemental Ratio Records for Benthic Foraminifera *Hoeglundina elegans*. Paleoceanogr. Paleoclimatol. 35, e2019PA003801.

Maier, E., Zhang, X., Abelmann, A., Gersonde, R., Mulitza, S., Werner, M., Méheust, M., Ren, J., Chapligin, B., Meyer, H., Stein, R., Tiedemann, R., Lohmann, G., 2018. North Pacific freshwater events linked to changes in glacial ocean circulation. Nature 559, 241–245.

Marchitto, T.M., Lehman, S.J., Ortiz, J.D., Flückiger, J., van Geen, A., 2007. Marine Radiocarbon Evidence for the Mechanism of Deglacial Atmospheric CO_2 Rise. Science 316, 1456–1459.

Marcott, S.A., Clark, P.U., Padman, L., Klinkhammer, G.P., Springer, S.R., Liu, Z., Otto-Bliesner, B.L., Carlson, A.E., Ungerer, A., Padman, J., He, F., Cheng, J., Schmittner, A., 2011. Ice-shelf collapse from subsurface warming as a trigger for Heinrich events. Proc. Natl Acad. Sci. USA 108, 13415–13419.

Marshall, J., Speer, K., 2012. Closure of the meridional overturning circulation through Southern Ocean upwelling. Nat. Geosci. 5, 171–180.

Max, L., Rippert, N., Lembke-Jene, L., Mackensen, A., Nürnberg, D., Tiedemann, R., 2017. Evidence for enhanced convection of North Pacific Intermediate Water to the low-latitude Pacific under glacial conditions. Paleoceanography 32, 41–55.

McManus, J.F., Francois, R., Gherardi, J.M., Keigwin, L.D., Brown-Leger, S., 2004. Collapse and rapid resumption of Atlantic meridional circulation linked to deglacial climate changes. Nature 428, 834–837.

Meehl, G.A., Arblaster, J.M., Fasullo, J.T., Hu, A., Trenberth, K.E., 2011. Model-based evidence of deep-ocean heat uptake during surface-temperature hiatus periods. Nature Clim. Change 1, 360–364.

Oppo, D.W., Fairbanks, R.G., 1989. Carbon isotope composition of tropical surface water during the past 22,000 years. Paleoceanography 4, 333–351.

Pahnke, K., Goldstein, S.L., Hemming, S.R., 2008. Abrupt changes in Antarctic Intermediate Water circulation over the past 25,000 years. Nat. Geosci. 1, 870–874.

Palmer, M.R., Pearson, P.N., 2003. A 23,000-year record of surface water pH and pCO$_2$ in the western equatorial Pacific Ocean. Science 300, 480–482.

Parker, F.L., Berger, W.H., 1971. Faunal and solution patterns of planktonic foraminifera in surface sediments of the South Pacific. Deep Sea Research and Oceanographic Abstracts 18, 73–107.

Poggemann, D.-W., Nürnberg, D., Hathorne, E.C., Frank, M., Rath, W., Reißig, S., Bahr, A., 2018. Deglacial Heat Uptake by the Southern Ocean and Rapid Northward Redistribution Via Antarctic Intermediate Water. Paleoceanogr. Paleoclimatol. 33, 1292–1305.

Praetorius, S.K., Condron, A., Mix, A.C., Walczak, M.H., McKay, J.L., Du, J., 2020. The role of Northeast Pacific meltwater events in deglacial climate change. Science Advances 6, eaay2915.

Rebotim, A., Voelker, A.H.L., Jonkers, L., Waniek, J.J., Schulz, M., Kucera, M., 2019. Calcification dept. of deep-dwelling planktonic foraminifera from the eastern North Atlantic constrained by stable oxygen isotope ratios of shells from stratified plankton tows. J. Micropalaeontol. 38, 113–131.

Riethdorf, J.-R., Max, L., Nürnberg, D., Lembke-Jene, L., Tiedemann, R., 2013. Deglacial development of (sub) sea surface temperature and salinity in the subarctic northwest Pacific: Implications for upper-ocean stratification. Paleoceanography 28, 91–104.

Ritz, S.P., Stocker, T.F., Grimalt, J.O., Menviel, L., Timmermann, A., 2013. Estimated strength of the Atlantic overturning circulation during the last deglaciation. Nat. Geosci. 6, 208–212.

Romahn, S., Mackensen, A., Groeneveld, J., Pätzold, J., 2014. Deglacial intermediate water reorganization: new evidence from the Indian Ocean. Clim. Past 10, 293–303.

Ronge, T.A., Frische, M., Fietzke, J., Stephens, A.L., Bostock, H., Tiedemann, R., 2021a. Southern Ocean contribution to both steps in deglacial atmospheric CO$_2$ rise. Scientific Reports 11, 22117.

Ronge, T.A., Lippold, J., Geibert, W., Jaccard, S.L., Mieruch-Schnülle, S., Süfke, F., Tiedemann, R., 2021b. Deglacial patterns of South Pacific overturning inferred from ^{231}Pa and ^{230}Th. Scientific Reports 11, 20473.

Rosenthal, Y., Linsley, B.K., Oppo, D.W., 2013. Pacific ocean heat content during the past 10,000 years. Science 342, 617-621.

Sagawa, T., Yokoyama, Y., Ikehara, M., Kuwae, M., 2011. Vertical thermal structure history in the western subtropical North Pacific since the Last Glacial Maximum. Geophys. Res. Lett. 38, L00F02.

Sánchez, A., Carriquiry, J.D., 2022. Millennial-scale marine productivity changes and the persistence of Antarctic intermediate water off Baja California, Mexico, during the last 6–60 kyr. Quat. Sci. Rev. 291, 107661.

Schiebel, R., Hemleben, C., 2017. Planktic Foraminifers in the Modern Ocean. Springer Berlin Heidelberg, Berlin, Heidelberg, Germany.

Schiraldi, B., Sikes, E.L., Elmore, A.C., Cook, M.S., Rose, K.A., 2014. Southwest Pacific subtropics responded to last deglacial warming with changes in shallow water sources. Paleoceanography 29, 2013PA002584.

Schlitzer, R., 2015. Ocean Data View 4, http://odv.awi.de.

Schmitt, J., Schneider, R., Elsig, J., Leuenberger, D., Lourantou, A., Chappellaz, J., Köhler, P., Joos, F., Stocker, T.F., Leuenberger, M., Fischer, H., 2012. Carbon Isotope Constraints on the Deglacial CO_2 Rise from Ice Cores. Science 336, 711-714.

Shackleton, N., 1974. Attainment of isotopic equilibrium between ocean water and the benthonic foraminifera genus *Uvigerina* isotopic changes in the ocean during the last glacial. Colloques Internationaux du C.N.R.S. 219, 203-209.

Siani, G., Michel, E., De Pol-Holz, R., DeVries, T., Lamy, F., Carel, M., Isguder, G., Dewilde, F., Lourantou, A., 2013. Carbon isotope records reveal precise timing of enhanced Southern Ocean upwelling during the last deglaciation. Nature Communications 4, 2758.

Spratt, R.M., Lisiecki, L.E., 2016. A late Pleistocene sea level stack. Clim. Past 12, 1079-1092.

Steph, S., Regenberg, M., Tiedemann, R., Mulitza, S., Nürnberg, D., 2009. Stable isotopes of planktic foraminifera from tropical Atlantic/Caribbean core-tops: Implications for reconstructing upper ocean stratification. Mar. Micropaleontol. 71, 1-19.

Stott, L., Southon, J., Timmermann, A., Koutavas, A., 2009. Radiocarbon age anomaly at intermediate water depth in the Pacific Ocean during the last deglaciation. Paleoceanography 24, PA2223.

Struve, T., Wilson, D.J., Hines, S.K.V., Adkins, J.F., van de Flierdt, T., 2022. A deep Tasman outflow of Pacific waters during the last glacial period. Nature Communications 13, 3763.

Talley, L.D., 2008. Freshwater transport estimates and the global overturning circulation: Shallow, deep and throughflow components. Progress in Oceanography 78, 257-303.

Tapia, R., Nürnberg, D., Ronge, T., Tiedemann, R., 2015. Disparities in glacial advection of Southern Ocean intermediate water to the south Pacific gyre. Earth

Planet. Sci. Lett. 410, 152-164.

Toggweiler, J.R., Dixon, K., Broecker, W.S., 1991. The Peru upwelling and the ventilation of the south Pacific thermocline. J. Geophys. Res.: Oceans 96, 20467-20497.

Toggweiler, J.R., Lea, D.W., 2010. Temperature differences between the hemispheres and ice age climate variability. Paleoceanography 25, PA2212.

Umling, N.E., Oppo, D.W., Chen, P., Yu, J., Liu, Z., Yan, M., Gebbie, G., Lund, D.C., Pietro, K.R., Jin, Z.D., Huang, K.F., Costa, K.B., Toledo, F.A.L., 2019. Atlantic Circulation and Ice Sheet Influences on Upper South Atlantic Temperatures During the Last Deglaciation. Paleoceanogr. Paleoclimatol. 34, 990-1005.

Wang, F., Zang, N., Li, Y., Hu, D., 2015. On the subsurface countercurrents in the Philippine Sea. J. Geophys. Res. Oceans 120, 131-144.

Weaver, A.J., Saenko, O.A., Clark, P.U., Mitrovica, J.X., 2003. Meltwater Pulse 1A from Antarctica as a Trigger of the Bølling-Allerød Warm Interval. Science 299, 1709-1713.

Wong, A.P.S., Bindoff, N.L., Church, J.A., 1999. Large-scale freshening of intermediate waters in the Pacific and Indian oceans. Nature 400, 440-443.

Xie, R.C., Marcantonio, F., Schmidt, M.W., 2012. Deglacial variability of Antarctic Intermediate Water penetration into the North Atlantic from authigenic neodymium isotope ratios. Paleoceanography 27, PA3221.

Yang, Y., Xiang, R., Zhang, L., Zhong, F., Zhang, M., 2020. Is the upward release of intermediate ocean heat content a possible engine for low-latitude processes? Geology 48, 579-583.

Yu, Z., Colin, C., Ma, R., Meynadier, L., Wan, S., Wu, Q., Kallel, N., Sepulcre, S., Dapoigny, A., Bassinot, F., 2018. Antarctic Intermediate Water penetration into the Northern Indian Ocean during the last deglaciation. Earth Planet. Sci. Lett. 500, 67-75.

Zhang, S., 2016. The Upper Water Body Structure Evolution in the Core Region of the Western Pacific Warm Pool and its Correlation to the ENSO-like Process and ITCZ Shift since MIS10, University of Chinese Academy of Sciences University of Chinese Academy of Sciences, p. 159.

Zhang, S., Li, T., Chang, F., Yu, Z., Xiong, Z., Wang, H., 2017. Correspondence between the ENSO-like state and glacial-interglacial condition during the past 360 kyr. Chin. J. Ocean. Limnol. 35, 1018-1031.

Zhang, S., Yu, Z., Gong, X., Wang, Y., Chang, F., Lohmman, G., Qi, Y., Li, T., 2021. Precession cycles of the El Niño/Southern Oscillation-like system controlled by Pacific upper-ocean stratification. Communications Earth & Environment 2, 239.

Zhang, S., Yu, Z., Wang, Y., Gong, X., Holbourn, A., Chang, F., Liu, H., Cheng, X., Li, T., 2022. Thermal coupling of the Indo-Pacific warm pool and Southern Ocean over the past 30,000 years. Nature Communications 13, 5457.

Zou, J., Shi, X., Zhu, A., Kandasamy, S., Gong, X., Lembke-Jene, L., Chen, M.T., Wu, Y., Ge, S., Liu, Y., Xue, X., Lohmann, G., Tiedemann, R., 2020. Millennial-scale variations in sedimentary oxygenation in the western subtropical North Pacific and its links to North Atlantic climate. Clim. Past 16, 387-407.

Zweng, M., Reagan, J., Seidov, D., Boyer, T., Locarnini, R., Garcia, H., Mishonov,

A., Baranova, O., Weathers, K., Paver, C., Smolyar, I., 2018. World ocean atlas 2018, volume 2: Salinity. NOAA Atlas NESDIS 82, 50.

Declaration of interest statement

The authors declare that they have no known competing financial interests or personal relationships that could have appeared to influence the work reported in this paper.

Highlights:

- We reconstructed the thermohaline and $\delta^{13}C$ variations of intermediate water in the equatorial Pacific over the past 28,000 years.
- The temperature of the Pacific intermediate water rose by ~6°C and accompanied by a salinity enrichment in Heinrich Stadial 1.
- The thermohaline and $\delta^{13}C$ of intermediate water show a temporal correspondence to Southern Ocean surface water.